Appl. Phys. B 58, 333–342 (1994)

Applied Physics B Lasers and Optics

Spatially Resolved Raman Scattering for Multi-Species and Temperature Analysis in Technically Applied Combustion Systems: Spray Flame and Four-Cylinder In-Line Engine

G. Grünefeld [1], V. Beushausen [1], P. Andresen [2], W. Hentschel [3]

[1] Laser-Laboratorium Göttingen, Im Hassel 21, D-37077 Göttingen, Germany (Fax: +49-551/503599)
[2] University of Bielefeld, Universitätsstrasse 25, D-33615 Bielefeld, Germany (Fax: +49-521/1065244)
[3] Volkswagen AG, Research and Development, D-38436 Wolfsburg, Germany (Fax: +49-5361/978794)

Received 24 June 1993/Accepted 29 October 1993

Abstract. Spatially resolved Raman scattering is used to measure the single shot stoichiometry before ignition inside a realistic internal combustion engine with high single shot precision of 1%–4% (depending on the extent of spatial averaging). The high precision results from the simultaneous detection of fuel and N_2 (O_2), which yields stoichiometry via a relative measurement. The cycle-to-cycle fluctuations of stoichiometry are clearly resolved. The feasibility of averaged spatially resolved simultaneous multi-species detection is demonstrated in a commercial oil-burning furnace as well. The limited precision that is usually obtained in Raman scattering by interfering emissions is highly improved using the fact that the interfering emission is unpolarized whereas Raman scattering is highly polarized. Therefore, Raman measurements provided good signal-to-noise ratios in the spray flame even in the area where fuel droplets occur and during combustion in the engine. The optical multichannel analyzer yields one-dimensional spatial resolution, and offers the capability to easily combine Raman scattering with Rayleigh scattering and laser-induced fluorescence detection of minority species.

PACS: 07.60, 35.00, 82.40

The great potential of spontaneous vibrational Raman scattering particularly in the deep UV for combustion diagnostics has been demonstrated recently in a number of laboratory flame experiments [1–5]. Nevertheless, only a few attempts were done to use this method in technically applied combustion systems [6, 7] because of the hostile experimental conditions in real combustion devices (droplets, soot, aromatic hydrocarbons). Spontaneous Raman scattering is particularly sensitive to interfering emissions from these concomitants of combustion due to its comparatively small signal levels [1, 8, 9]. The application of Raman scattering for the diagnostics in a production-line oil-burning furnace and an automobile engine that is demonstrated in this work is only successful because high power UV lasers are used: Raman scattering intensity scales with the fourth power of the laser frequency. This yields a sufficient signal-to-noise level and allows precise multi-species measurements, e.g. for stoichiometry determination inside an internal combustion engine.

The selective species detection by Raman scattering requires high discrimination against underlying broadband laserinduced fluorescence in the combustion of hydrocarbons. This discrimination is attained using polarization properties, i.e. by rotating the electric vector of the laser light and measuring the LIF background separately. Although the polarization of Raman and Rayleigh scattering are well known and used extensively to analyze molecular structure [22], only some early attempts have been made to use it to eliminate the interfering laser induced emission in combustion [1 and references therein].

In contrast to other laser spectroscopic techniques (LIF, CARS) linear Raman scattering offers some important advantages: 1) simultaneous spatially resolved measurements of partial densities of all majority species, 2) simultaneous spatially resolved temperature measurements (for example via Stokes and anti-Stokes ratios of nitrogen), 3) substantially easier quantification [1, 8], 4) in a number of important cases, e.g. temperature and fuel/air ratio measurements, it is unaffected by laser power fluctuations and transmission properties of optics (i.e. dirtying of windows by oil, soot etc. particularly in engines, which attenuates emissions at all wavelengths equally) because a *ratio* of two simultaneously acquired spectral lines is used.

Spatial resolution is particularly vital for the analysis of complex turbulent combustion systems because gradients of state properties can be measured. The Optical Multichannel Analyzer (OMA) yields not only spectral information but also one-dimensional spatial resolution along the line of the focused laser beam. In the spectral direction an entire emission range can be recorded with each laser shot, which also offers the possibility to combine Raman scattering with Rayleigh (and Mie) scattering and Laser Induced Fluorescence LI(P)F.

Recently such spatially resolving OMA systems were applied to the study of hydrogen flames [5, 10]. In the present case of hydrocarbon combustion much higher background luminosity cause much bigger problems.

Both combustion devices in this report have previously been used in other studies [11–13]. To our knowledge, these are the first applications of spatially resolved Raman scattering to a spray flame (in the area of droplets) and to a realistic four-cylinder internal combustion engine. Previous linear Raman scattering measurements in internal combustion engines are very rare and were applied only to one-cylinder model engines using gaseous fuel [14, 15]. These approaches used 532 nm lasers and therefore needed large collection solid angles (with magnifying optics) and a big observation window in the (or instead of the) cylinder head. In the present setup the collection solid angle can be considerably smaller (5×10^{-3} sr) because a deep UV laser is used. This allows a) more realistic engines, b) large polarization effects (which turn out to be vital using liquid fuel), and c) simultaneous observation of a long line (45 mm) across the cylinder (at a given aperture of the spectrograph and photocathode diameter). Only one study is known that used a spatially resolving OMA system for detection of Raman scattering inside an engine [14] (the lenght of the observed spatial line was 15 mm. The authors concluded that it was not possible to do quantitative single shot measurements at all because of weak signals and since a TV camera was used. No cycle-to-cycle fluctuations in the compression stroke could be resolved because of large standard deviations of the technique (stoichiometry variations were not expected anyway because premixed propane/air was used). Interference problems from oil fluorescence arose after ignition.

In this work the use of a UV laser (and a CCD camera) makes it possible to achieve a noise level of a few percent for single shots in the compression stroke (depending on the species and the extent of spatial averaging). Therefore, cycle-to-cycle fluctuations of the stoichiometry and exhaust gas content in the initial load are clearly resolved.

Averaged measurements from the combustion and exhaust stroke in the engine and from different positions in the spray flame are presented, too. Even without quantification (and despite the inherent errors that are obtained from averaged Stokes/anti-Stokes temperature measurements in turbulent media) these multi-species and temperature data with a good signal-to-noise ratio may be valuable information for the understanding and optimization of combustion devices, as demonstrated in an earlier paper [13].

1 Experimental

The experimental setup at the oil-burning furnace (produced by the german company Viessmann) is outlined in Fig. 1. A horizontal spray flame (about 30 cm long) is generated by a fuel/air mixing device consisting of a fuel injector nozzle and a baffle plate with 4 radial slits (diameter 58 mm). This causes a turbulent vortex structure of the flame. More details of the furnace are given in [13]. The boiler is modified for optical access by the quartz windows 1, 2, and 3. Isooctane (C_8H_{18}) is used as liquid fuel because it does not absorb the excimer laser wavelength. The fuel/air mixing ratio is nearly stoichiometric (equivalence ratio = 0.95). The laser beam is focused by a spherical lens ($f = 1$ m) and directed perpendicularly through the spray flame. The focus is located several centimetres behind the flame to avoid ignition and gas breakdown in the probe area. Since the furnace is mounted on a moveable table every spatial position of the flame can be investigated without realigning optics. A 50 mm long section of the focussed laser beam in the flame is imaged onto the entrance slit of a spectrograph (ISA Jobin-Yvon H-25, aperture $f/3.5$, resolution 0.3 nm) by a spherical lens ($f = 150$ mm) with a demagnification of 4:1. An image-intensified Peltier-cooled CCD camera (La Vision) is mounted in the exit plane of the spectrograph. One dimension of the CCD-chip (384 columns) corresponds to the spectral axis while the other one (286 rows) yields spatial resolution along the imaged section (50 mm).

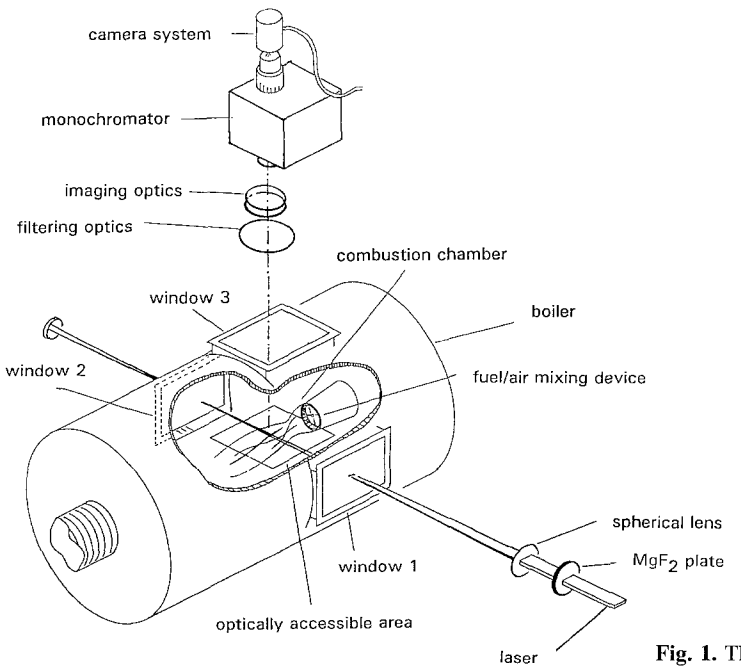

Fig. 1. The experimental setup at the oil-burning furnace

The spatial resolution is limited by the 2 mm height of the laser beam in the direction of observation. The spatial resolution along the laser beam axis was determined empirically to be at least 0.5 mm by analyzing the intensity change along this direction associated with an illuminated object in the focal plane.

The width of the probe volume (0.8 mm) is determined by the demagnification and the entrance slit of the spectrometer (0.2 mm). Since the laser beam is about 5 times wider than the imaged probe volume the photon flux seen by the spectrograph hardly depends on small alterations of the laser adjustment. This is important for quantitative measurements in the part of the spray flame containing droplets because these can cause beam steering effects due to refraction. Even if such effects are present temperature measurements are still precice since the ratio of Stokes and anti-Stokes lines is unaffected. However, negligible refraction effects were observed in the beam profile behind the furnace, even when the laser beam passed the droplet contaminated area close to the fuel nozzle.

The slow scan signal from the CCD camera is acquired and digitized by a personal computer system (dynamic range 12 bit). The image-intensifier is gated (200 ns) to reduce flame luminosity.

The laser source is a tunable narrowband KrF excimer laser (Lambda-Physik EMG 160 MSC) generating about 200 mJ per pulse at 248 nm (pulse length about 25 ns). This laser was optimized regarding locking efficiency, linear polarization, and beam profile. These three features are imperative for a successful application, as described below. Essentially the laser was modified in the following way: The amplifier is used in a single-pass configuration. A 2 mm slit (instead of the commercial pin hole) is located before the output mirror of the oscillator. The oscillator beam is broadened prior to reaching the amplifier by an additional path length of 2 m so that it includes the entire volume of the amplifier discharge (width of about 5 mm) [16]. This combines the high output power of the commercial configuration with better locking efficiency, beam profile, and degree of polarization of the (unmodified) single-pass. Narrow bandwidth and a high locking efficiency is needed to avoid LIPF interference of OH and O_2 occurring in the tuning range of this excimer around 248 nm [17], which would make a quantitative analysis of Raman signals impossible. Usually a wavelength of 248.62 nm is used for the measurements, where only a small amount of O_2 LIPF was observed in the flames due to remaining broadband emission of the laser [4, 17]. A high degree of linear polarization of the laser light (here better than 95%) is advantageous when the polarization properties of vibrational Raman scattering are used to discriminate against interfering laser induced fluorescence. The underlying broadband LIF from aromatic hydrocarbons is known to cause serious interference problems for Raman measurements in turbulent hydrocarbon flames. However, the interfering emission can be discriminated against Raman scattering by polarization techniques, i.e. by rotating the electric vector of the laser radiation with respect to the detector. Whereas the interfering emission is generally depolarized vibrational Raman scattering is highly polarized, with the degree of polarisation depending on the type of molecule (and vibrational mode). The remaining O_2 LIPF is eliminated in the same way. In the experiments a simple birefringent MgF_2-plate is used to rotate the electric vector of laser light. For rapid "switching" of the E-vector direction during measurement the angle of the plate with respect to the beam direction is adjusted by a computer controlled step motor. A half-wave plate (248 nm) in front of the spectrograph optimizes the transmission of Raman (and Rayleigh) scattered light because the reflection of the grating is different for both polarization directions (this also helps to discriminate Raman scattering against LIF since it partly acts as a polarizer).

Two types of filters are used to attenuate Rayleigh and Mie scattered intensities in these experiments. Dielectric mirrors (0°) with a bandwidth of about 20 nm centered around 250 nm allow to observe both Stokes and anti-Stokes lines. Unfortunately the vibrational Raman bands of O_2 and CO_2 (in the region 256 nm to 259 nm) are also suppressed by such a filter. For simultaneous detection of these species a long-pass liquid butyl acetate filter is used instead of the dielectric mirrors. It has a very steep cut off in the region from 250 nm to 255 nm and blocks the anti-Stokes side completely. Because of strongly interfering Mie scattered light from fuel droplets in the spray flame experiments both Mie and Rayleigh scattering was simply suppressed by a piece of tape at the photocathode of the image-intensifier at the spectral location where scattered laser light appears on the camera.

The laser beam profile is much more homogeneous than that generated by the commercially available type of laser optics (Cassegrain). This is advantageous not only for imaging purposes, but also for applications when a focused laser beam is used like in these experiments. An inhomogeneous beam profile leads to "hot spots" after focussing and can therefore cause a) enhanced multi-photon processes (e.g. air breakdown, OH production from H_2O dissociation) b) destruction of optical components, e.g. the entrance and exit windows of the combustion chambers.

The latter is especially important for the second application described in this report, i.e. the internal combustion engine. Here, the laser beam passes through two thick quartz windows in the upper part of the cylinder, as is shown in the longitudinal section in Fig. 2. In these experiments the laser beam is focused by a spherical lens ($f = 2$ m), so that the beam waist is located outside the cylinder a few centimetres behind the exit window. The power density at the windows (used beam profile: 1.5 mm (width) × 3 mm (height) with 140 mJ/pulse) is close to the limit of destruction (about 4 J/cm^2 per pulse) to achieve high photon flux inside the cylinder, which is necessary for single shot measurements with high precision. The four-cylinder spark ignition engine (Volkswagen AG) has been described in more detail in earlier publications [11, 12]. The measurements described below were carried out at 1400 rpm, 40 Nm load and a stoichiometric (in average) fuel/air mixture with isooctane as fuel. Optical access for the spatially resolving OMA system is through the piston window and a fixed mirror as shown in Fig. 2. A 4.5 cm section along the laser path in the cylinder is imaged onto the entrance slit of the spectrograph by a pair of spherical lenses ($f_1 = 250$ mm, $f_2 = 300$ mm). The spectrograph used is an Oriel Multispec (aperture $f/3.7$). Single shot as well as averaged measurements were done at selected

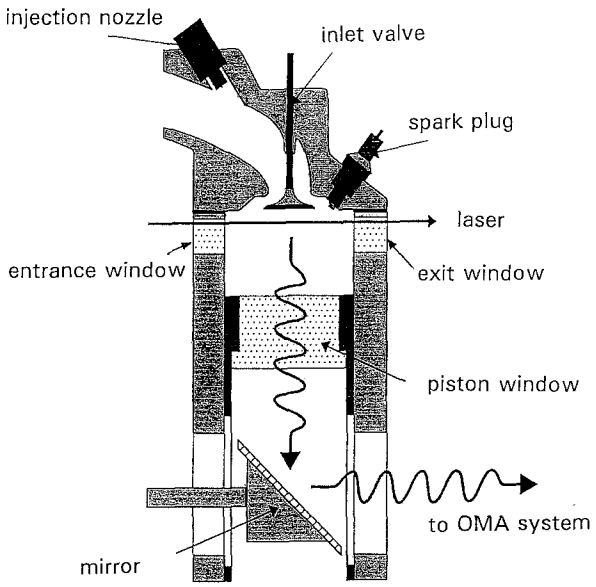

Fig. 2. Longitudinal section of the fourth cylinder of the spark ignition engine modified for optical access

crank angles of the four-stroke cycle. Averaged image acquisition is done by on-chip integration, i.e. adding images from multiple laser pulses (one pulse per cycle) during one CCD integration time.

2 Results from the Spray Flame

Figure 3a–c show three typical raw images that appear at the camera if it is mounted in the image plane of the spectrograph for the case of the liquid spray flame in the furnace. The images were acquired by averaging over 1000 laser shots in three different positions in the central plane of the flame: (a) 1 cm, (b) 6 cm, and (c) 16 cm behind the baffle plate of the fuel/air mixing device. As discussed in an earlier publication at these high shot numbers the distributions are precicely reproducible despite the turbulent combustion [13]. The images represent three very different zones dominated by: (a) fuel/air injection and droplet evaporation, (b) turbulent combustion, and (c) exhaust gas. Obviously there are great spatial and spectral differences between the raw images. (The conversion of intensities to colours is given by the colour bar at the right sides of each image. Different false colour tables were applied for the images in Fig. 3 for better visibility so that the absolute intensities cannot be compared. However, the intensities in the corresponding spectral plots in Fig. 4 can be compared.)

The vertical axis of the images (Fig. 3a–c) corresponds to a 50 mm long line across the flame around its middle axis. The laser wavelength appears roughly in the middle of the images (i.e. at 248 nm) so that the anti-Stokes side from 225 nm to 239 nm as well as the Stokes side from 260 nm to 280 nm can be observed. The emission in the vicinity of the laser line is suppressed by a black stripe and two additional dielectric filters. Intense broadband laser induced fluorescence occurs at the Stokes side and – to a much smaller extent – also in the anti-Stokes region. This emission most probably originates from pyrolysis products of fuel [13]. Despite the comparatively large signal strength at the deep UV frequency one of the major problems for the use of Raman scattering in hydrocarbon flames – the difficult discrimination against interfering emission – becomes obvious here. The spatial distribution of this broadband LIF emission varies strongly with the position in the flame: Two maxima are present in the first image caused by two of the four slits in the baffle plate of the fuel/air mixing device, where most of the fuel droplets are injected. The different intensities on the maxima indicate that the flame is not perfectly symmetric [13]. At 6 cm distance from the baffle plate (Fig. 3b) a single cone of fuel/air vapor is seen. At 16 cm (Fig. 3c) the broadband emission is less intense and more homogeneous.

The occurrence of the broadband LIF roughly spatially coincides with the Raman emission from fuel (C_8H_{18} and other hydrocarbons, spectral region from 267.5 nm to 268.4 nm). The other more intense vibrational Raman emissions in the images are from nitrogen (Stokes at 263.8 nm and anti-Stokes at 233.4 nm) and water (asymmetric stretch mode at 273.3 nm). The Stokes Raman bands of O_2 and CO_2 are not observed in these measurements because of spectral filtering. Whereas nitrogen is detected allover the flame the water emission appears with high intensities only in the Figs. 3b, c, where combustion is active. In most parts of the flame (here Fig. 3b) water and hydrocarbons, i.e. products and educts, can be detected simultaneously due to the turbulent combustion behaviour.

The nitrogen anti-Stokes intensity increases in the sequence of Fig. 3a–c due to rising temperature. In fact its magnitude is too small for temperature calculation from the Stokes/anti-Stokes ratio in the first few centimetres of the flame because the temperature is well below 1000 K.

Calibration of the temperature measurements via nitrogen Stokes/anti-Stokes ratios is performed using (a) a hot air blower (1100 K) and (b) the exhaust gas of a laminar premixed CH_4 flame (2100 K). Both devices can be mounted inside the oil-burning furnace. The absolute temperatures of the calibration devices are measured via the decrease of the nitrogen Stokes signal in the (exhaust) gas in comparison to room air. Quantitative temperature profiles will be given in a forthcoming paper because the evaluation of the data (as described in the appendix) is not yet finished. The measurement precision is estimated to be about 5% at distances larger than 5 cm behind the nozzle.

In the image *c* the particle and temperature distributions are nearly homogeneous. The remaining vertical differences are partly caused by pixel dependent gain and spatially resolved sensitivity of the OMA system. A "white image" could be used for correction or the species could be calibrated one by one acquiring images under homogenous conditions, e.g. room air for N_2, O_2, and H_2O [10].

For quantitative measurements of particle densities and temperatures discrimination against the underlying laser-induced fluorescence is of great importance for selective species detection. Figure 4 gives spectral intensity profiles calculated from the images in Fig. 3a–c by averaging over one half of the spatial axis of the images centered around the middle (different ordinate scales in Fig. 3a–c should be noticed). The two curves (E^H, E^V in Fig. 4a–c are for differ-

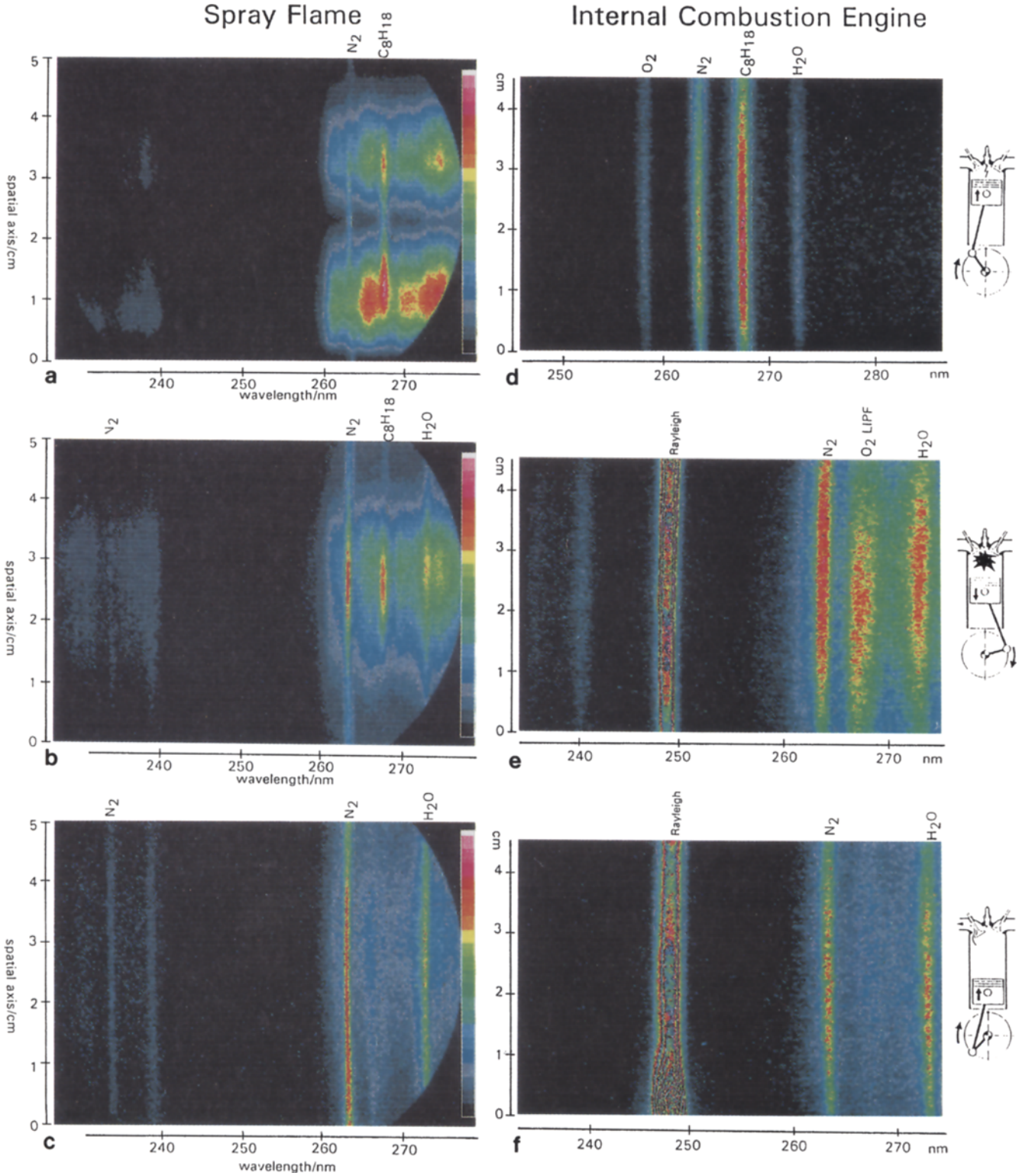

Fig. 3a–f. Averaged raw images from the oil-burning furnace (**a–c**) and the spark ignition engine (**d–f**). Image **a** was acquired 1 cm (b: 6 cm; c: 16 cm) behind the baffle plate of the fuel/air mixing device. Image (**d**) was recorded 30° before top-dead-center in the compression stroke, (**e**) at crank angle 30° after top-dead-center in the expansion stroke, and (**f**) at crank angle 180° at the beginning of the exhaust stroke

ent orientation of the electric vector of the linearly polarized laser radiation. It can be seen that Raman intensities and LIF occur in roughly comparable extent. Linear interpolation of the broadband LIF from both sides of each Raman branch will hardly result in high precision because the underlying emission shows pronounced curvature at this spectral resolution. However, exact determination of LIF underlying a Raman branch can be achieved by rotating the electric vector of the laser light. This was done for measurements shown in Fig. 3a–c and the results are plotted in Fig. 4 as a second

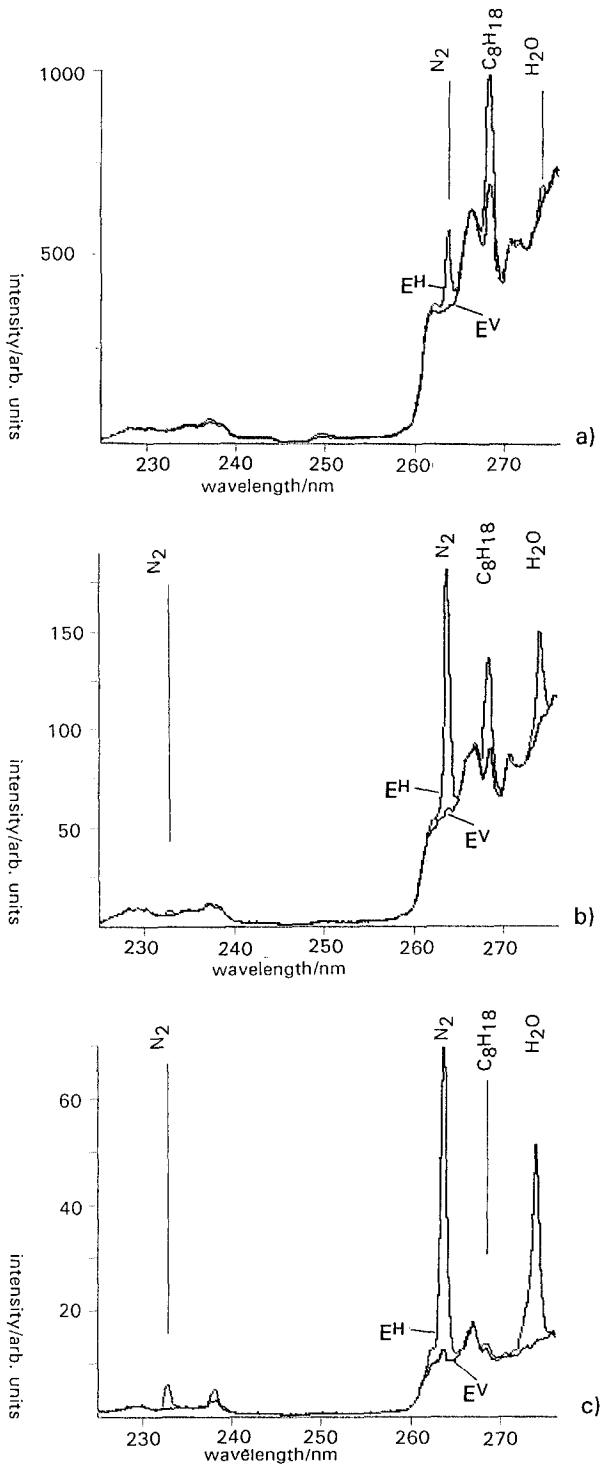

Fig. 4a–c. Spectral profiles calculated from the images in Fig. 3a–c by averaging over one half of the spatial range centered around the middle. Image (**a**) was acquired 1 cm behind the fuel/air mixing device, (**b**) at a distance of 6 cm, and (**c**) at 16 cm. The second curve in each panel results from a measurement with parallel E-vector of the laser light with regard to the camera axis

graph in each panel. The result indicates that the underlying LIF is depolarized whereas Raman scattering is polarized. This is the method that allows selective species detection of majority species even under severely interfering emissions as for liquid spray flames.

The extent of Raman depolarization depends on the type of molecule and vibrational mode and must be taken into account for quantification. For example the water branch disappears almost completely while nitrogen decreases by only a factor of about 7 with E^{H} compared to E^{V}. This factor can be determined in room air, but the appropriate value may be different for flame temperatures due to different contributions from Q and O/S branches. Ignoring this effect errors will be obtained in the determination of densities, but this is avoided by an easy calibration procedure and some calculations, which is described in the appendix. If the temperature is known (from Stokes/anti-Stokes ratio) the variation of the overall cross-section for the integrated Raman branch can be easily calculated from $(v+1)$-scaling of the vibrational contributions for a diatomic molecule [8]. So it is not absolutely necessary to measure temperature-dependent calibration curves in the case of nitrogen (and oxygen).

The situation is much more complicated in the case of fuel detection under flame conditions. The observed line from 267.5 nm to 268.4 nm consists of the C–H stretch mode, the degenerate vibrations of the CH_3– group, and other contributions depending on the type of hydrocarbon [18]. When fuel is affected by pyrolysis the line shape and polarization behaviour changes as a result of the formation of other hydrocarbon molecules. This is observed in images like Fig. 3a at slightly improved spectral resolution by comparing the line shape *in* and *between* the two areas of maximum fuel occurrence: between these areas the line peaks are more red shifted. This can be explained by pyrolysis because the break-up of C_8H_{18} favours the CH_3– line at 268.3 nm. (Besides that the C–H stretch mode can change its spectral profile between 267.5 nm and 268.4 nm depending on the prevailing molecular structure [18]).

Another consequence of pyrolysis is the alteration of polarization dependency. In Fig. 4b the "attenuated" Raman profile peaks are red shifted. This observation can be explained by enhanced CH_3– vibrational intensity, too, since this line is totally depolarized in contrast to the C–H mode [18]. So both features, i.e. line shape and polarization behaviour, are a consequence of pyrolysis and can be applied as a qualitative marker for this process. Before pyrolysis occurs quantification is easy because the integral vibrational cross-section hardly changes. Quantitative profiles will be given in a later publication.

It should be noticed that some laser-induced predissociative fluorescence from O_2 ($v=6,7$) is present in Fig. 3b, c [13]. It appears around 267 nm on the Stokes and around 239 nm (together with O_2 and CO_2 Raman) on the anti-Stokes side [17]. It partly interferes with hydrocarbon Raman scattering at this resolution, but it is discriminated by E-vector rotation since it is completely depolarized.

3 Results from the Automobile Engine

Deep UV spontaneous Raman scattering as with tunable excimer lasers turns out to be an ideal tool for the study of internal combustion engines because the main disadvantage of this technique, small cross-sections, is partly compensated by high particle densities. Even with small detection solid

angles as in these experiments (about 5×10^{-3} sr) spatially resolved single shot measurements are possible. Both single shot and averaged measurements are given below.

Despite the cycle-by-cycle instabilities of the combustion in Otto engines averaged measurements turn out to be fairly reproducible even if only about ten laser shots are integrated. Figure 3d–f display three averaged measurements at special crank angles from the compression (d), expansion (e), and exhaust stroke (f) of the four-stroke cycle. The first image (d) was integrated over ten cycles (one laser pulse per cycle) at crank angle 690°, i.e. 30° before top-dead-center in the compression stroke. Ignition takes place at this crank angle, but the flame front does not yet reach the probe area. The laser was adjusted near the top end of the windows across the middle axis of the cylinder. So the spatial axis represents 45 mm symmetric to the cylinder axis near the cylinder head.

A liquid butyl acetate filter (10 mm thick) was used for suppression of Rayleigh scattered light in the measurements in the compression stroke (Fig. 3d) so that O_2 vibrational Raman scattering is just slightly attenuated. Not only air, i.e. N_2 and O_2, and fuel vapour (C_8H_{18}) are observed, but also considerable quantities of H_2O. Some of it originates from residual exhaust gas of the preceding cycles (a portion of the exhaust gas remains in the cylinder mainly due to the clearence volume). The surprisingly high amount of water intensity will be discussed in a forthcoming paper. Another consequence of the presence of exhaust gas constituents is a small amount of broadband LIF occurring in Fig. 3d, which is probably caused by (aromatic) hydrocarbons. This can be seen more clearly in the emission spectrum in Fig. 5a, which was computed from Fig. 3d by averaging over the entire spatial range. The second graph in the profiles shows again the effect of E-vector rotation of the laser light and proves the existence of some underlying depolarized broadband emission. Because of the presence of exhaust gas some Raman scattered light from CO_2 is also expected at the short wavelength side of the O_2 Raman branch. However, it is too weak to be seen in Fig. 3d, partly because it is suppressed by the filter.

It should be emphasized that the hydrocarbon Raman intensity is much easier to convert to an absolute fuel density than for the spray flame because no pyrolysis occurs in the internal combustion engine before ignition.

Measurements after ignition are shown in Fig. 3e, f. They were averaged over 50 shots because the signal levels are smaller and less reproducible than late in the compression stroke. Here a dielectric filter was used to suppress the Rayleigh line for simultaneous observation of the Stokes and anti-Stokes sides. The Rayleigh line can be seen in the left half with high intensity. Figure 3e was acquired at crank angle 30° after top-dead-center in the expansion stroke, just when the flame front passed the probe volume. Nitrogen Stokes- and anti-Stokes signals are detected that could be used for temperature determination. The Raman band of water, which was produced by the combustion, appears very broad (see Fig. 5b) due to high temperature (>2000 K) [19]. The third prominent emission on the Stokes side shows little spatial dependence. It is caused by unburnt oxygen (broadband LIPF) and, to a much smaller extent, by hydrocarbons (Raman). In principle, both components could be roughly separated by E-vector rotation even at this

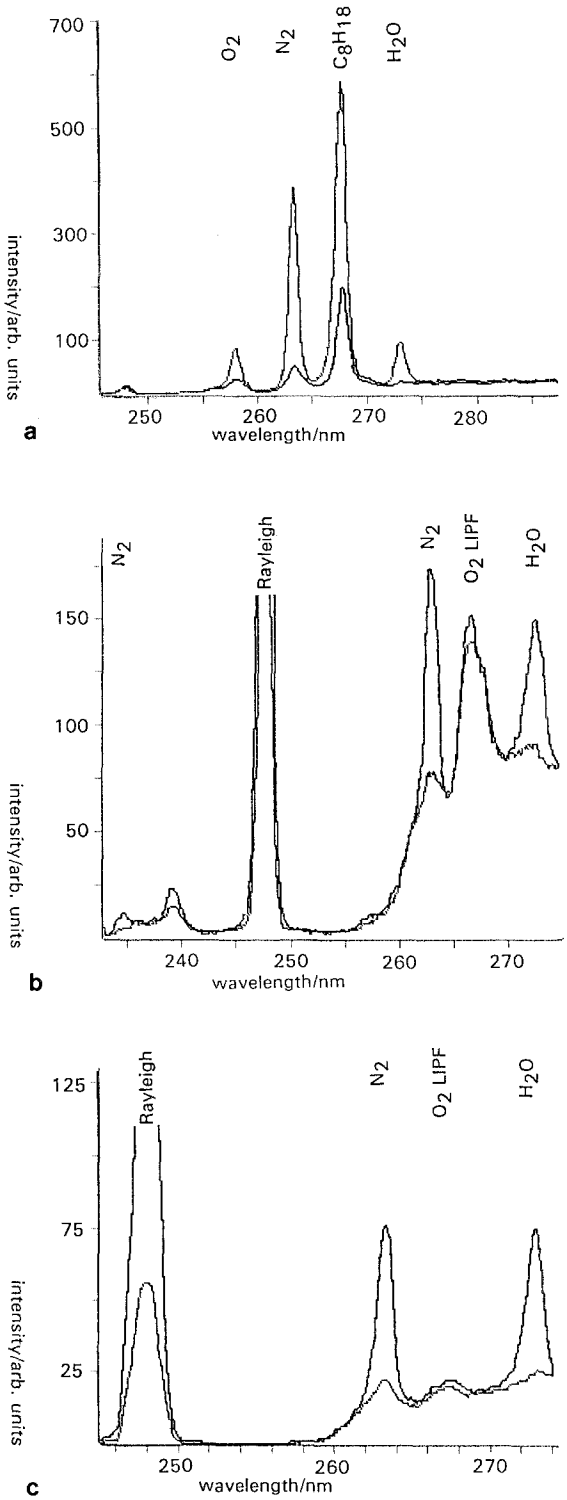

Fig. 5a–c. Spectral profiles computed from the raw frames Fig. 3d–f, which were acquired in the internal combustion engine during the compression stroke (**a**), the expansion stroke (**b**), and the exhaust stroke (**c**). These profiles were averaged over the entire spatial extension of the images

low spectral resolution (see above), but the oxygen LIPF is not very well reproducible with these small shot numbers. This is explained by the fact that the LIPF detection of high vibrational states ($v = 6$ and 7) depends on density *and* temperature fluctuations. That results in certain deviations

between the curves for both E-vector directions in Fig. 3e on the exact position of O_2 LIPF. The second line on the anti-Stokes side consists of O_2 LIPF and Raman scattering from O_2 and CO_2. It is therefore partly depolarized. Quantitative data will be given in forthcoming papers (particularly crank angle dependent behaviour of majority species and temperature during the exhaust stroke).

One main problem in the application of Rayleigh scattering in combustion engines is the discrimination against light scattering from the combustion chamber walls and windows [12, 20]. This difficulty can be solved by rotating the electric vector of the laser radiation, too, since the elastically scattered light from the walls is depolarized in contrast to Rayleigh scattered light. In these measurements the intensity on the Rayleigh line differs by a factor of about 5 when the E-vector direction is changed. The suppression should be sufficient for discrimination. Thus Rayleigh (and Mie) scattering can be used as complementary information, e.g. for temperature determination in special cases [12] or for the detection of droplets in the intake stroke. Figure 3e demonstrates the great flexibility of the spatially resolving OMA system that allows to use Raman-, Rayleigh- and LI(P)F methods simultaneously to gain multiple different information in complex situations.

Figure 3f was recorded at the bottom-dead-center (crank angle 180°) at the beginning of the exhaust stroke. The Stokes Raman bands of nitrogen and water are prominent here. The O_2 LIPF intensity and broadband LIF are decreased considerably in comparison to crank angle 30° due to the almost complete combustion. (The ordinate scales of the plots in Fig. 5 can not be compared quantitatively because the measurements were done under slightly different experimental conditions.)

It is well known that the spatial distribution of the fuel/air ratio just before ignition is of vital importance for the quality of the subsequent combustion stroke. To our knowledge, the data presented below are the first precise spatially resolved measurements of the fuel/air ratio for single combustion cycles in an internal combustion engine. Recent two-dimensional fuel visualization experiments using tracer substances indicate certain variations in the spatial distribution of the stoichiometry from cycle to cycle [21]. However, this technique does not measure the density of air simultaneously and therefore the fuel/air ratio can only be derived under additional assumptions, which may be incorrect due to cyclic variations in the engine operation (for example residual gas contents) and pulse-to-pulse aberrations of the measurement system.

On the contrary, spontaneous Raman scattering as it is used here with the spatially resolving OMA technique allows to measure fuel and air (and exhaust gas) simultaneously with spatial resolution along a line. This technique offers high precision because the stoichiometry is obtained as ratio of Raman intensities for fuel and N_2 (or O_2), i.e. the stoichiometry is derived from a relative measurement that eliminates most of the fluctuations caused by the measurement system, i.e. single shot laser power, laser adjustment, transmission of optics etc. As the Raman intensities of fuel (C_8H_{18}) and N_2 are comparable, the precision for the fuel/air equivalence ratio (close to unity) is dominated by the shot noise of the nitrogen signal alone. In the present experimental setup it is possible to achieve a shot noise level of N_2 at the crank angle of ignition (690°) of about 1% for single shots if one third (i.e. 15 mm) of the spatial extension is used for averaging (or 4% shot noise for 1 mm spatial resolution). Further improvements of the signal levels could be achieved using a larger detection solid angle or multi-pass configurations for the laser beam.

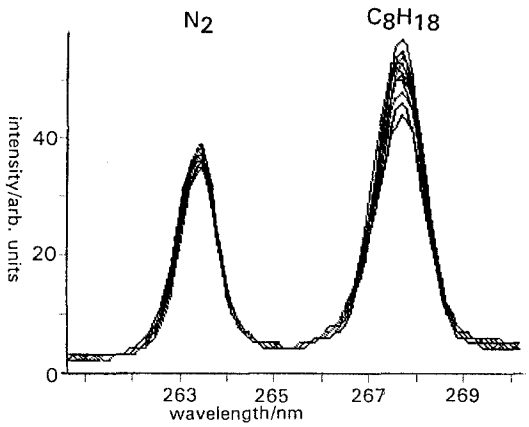

Fig. 6. Spectral profiles of fifteen single shots acquired at 30° before top-dead-center in the compression stroke of the combustion engine

The emission spectra in Fig. 6 show the N_2 and C_8H_{18} Raman emissions from 15 single shots at crank angle 690° averaged over the whole spatial range (45 mm). Spatial averaging results in a photon statistical error of less than 1% for the single shot N_2 signal, so that the spectral emission line shapes in Fig. 6 are highly reproducible for each laser shot in contrast to the absolute intensities. However, the important feature is that the variations in fuel intensity (integrated over the entire spectral width of the fuel emission) is considerably higher than of nitrogen (here: $\mathrm{rms}(C_8H_{18}) = 7.5\%$, $\mathrm{rms}(N_2) = 3.5\%$). The fluctuations of the N_2 intensity may be almost completely caused by variations of the single pulse laser power and not by cyclic variations in the load. In contrast, the increased fluctuation of the fuel intensity is obviously caused by real fluctuations of the mixture in the probed spatial area. In fact the resulting standard deviation of the fuel/air ratio in this measurement is $\mathrm{rms}(N_2/C_8H_{18}) = 7\%$. ($N_2$ is used here instead of O_2 because of higher signal level neglecting a small amount of present exhaust gas.)

It should be mentioned that the fluctuations in the measurement of the N_2 Raman signal – caused by the instability of the pulse-to-pulse variation of the laser power – do not affect the stoichiometry: These fluctuations are eliminated by the division of the Raman signals of fuel *relative* to N_2. This implies that the stoichiometry before ignition can be obtained on a single shot basis with a precision high enough to resolve the cycle-to-cycle fluctuations in Otto engines.

Correlations of the measured fuel/air ratio to the pressure curve have been obtained within in the same cycles. (The pressure over crank angle curve is simultaneously measured and gives a rough image of the combustion course of each cycle). This indicates the potential of this technique to investigate the influence of fuel/air mixture formation on the combustion process. Details of such measurements will be given in a later publication.

4 Summary and Conclusions

The results of this study prove that selective multi-species detection and temperature determination using spontaneous Raman scattering is possible even in the hostile environments of commercial spray flames and spark ignition engines. Compared to other laser diagnostic techniques linear Raman scattering with tunable KrF-excimer lasers and spatially resolving optical multichannel analyzers has the capability to measure densities of several majority species and temperatures simultaneously with spatial resolution along a line.

The use of Raman scattering in laser diagnostic applications is usually limited to relatively clean combustion environments because otherwise the weak signal can not be separated from the strong interfering emissions. It is demonstrated here that the interference problems can be solved by the use of polarization techniques even under the severe conditions in a liquid fuelled spray flame. It is interesting to note that it is possible to discriminate the Raman signal against interfering emission also on a single shot basis by separating the polarization components perpendicular and parallel to the E-vector.

The polarization properties are also used to discriminate(a) Raman scattering against LIPF from O_2 (excited at 248 nm) and(b) Rayleigh scattering against laser light that was elastically scattered by the combustion chamber walls and windows. This implies that Rayleigh scattering and LI(P)F detection (of OH and NO for example) can be simultaneously used as sources of complementary information.

Averaged measurements in the oil-burning furnace can be used for the comparison (and consecutive optimization) of different flame forms generated by various fuel/air mixing devices (and exhaust gas recirculation methods) because they are highly reproducible and sensitive on such technical variations. Previous work dealing with LI(P)F detection of minority species demonstrated that even qualitative data can be sufficient for this purpose [13].

In the internal combustion engine even single shot measurements are possible due to high particle densities. This allows to study cycle-by-cycle variations on a single shot basis besides averaged measurements. One challenging aim of future work is to observe correlations of fuel/air mixture formation with cycle-by-cycle fluctuations of the combustion process, i. e. pressure trace, flame front propagation, NO production etc.

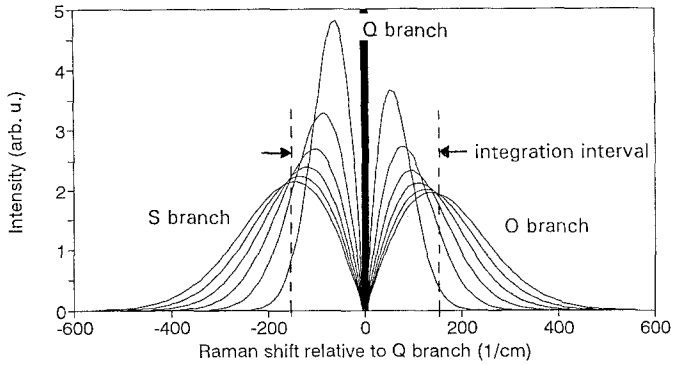

Fig. 7. Calculated spectral shapes of (unresolved) N_2 Stokes O and S branch intensities for $T = 300$, 900, 1200, 1500, 1800, and 2100 K (identical particle numbers)

Appendix
Density and Temperature Determination Procedure

Densities of diatomic molecules (N_2, O_2 etc.) are determined from OMA spectra by integrating the whole Q branch emission spectrum. The use of low-resolution spectrographs for multi-species detection has the disadvantage that the Q branch can not be separated from the O/S branches, which is easier with higher-resolution spectrographs. On the other hand, it is not useful to integrate the entire O/S branches because they are spread over a wide spectral range especially at flame temperatures and interference problems with other Raman lines may occur. Thus a useful spectral integration interval includes the entire Q branch and a certain fraction f of the O/S branches. This fraction is temperature dependent, i.e. $f = f(T)$, since O/S branches become wider with increasing T. Figure 7 shows theoretical spectral shapes of (unresolved) Stokes O and S branches of N_2 for different temperatures and a typical integration interval.

If the pure Raman signal is discriminated against underlying LIF emission by rotating the E-vector of the laser light by 90° the Q branch is suppressed by a factor p in contrast to the O/S branches that are totally depolarized. Thus most of the Raman emission with the E-vector parallel to the camera axis results from the O/S branches (particularly in normal room air). The signals for both E-vector directions integrated over the above mentioned spectral interval consist of three parts:

$$E^{\mathrm{H}} = \mathrm{LIF} + fOS + Q\,, \tag{A1}$$

$$E^{\mathrm{V}} = \mathrm{LIF} + fOS + Q/p\,. \tag{A2}$$

(LIF is the underlying LIF emission, OS the entire O/S branch intensity, and Q the Q branch intensity.) The factor p must be determined for the calculation of the Q branch intensity:

$$Q = (E^{\mathrm{H}} - E^{\mathrm{V}})/(1 - 1/p)\,. \tag{A3}$$

Since p depends not only on molecular constants but also on the measurement system (polarization of laser light, collection solid angle) it must be determined from a calibration procedure. This is done with room air for N_2 and O_2 by acquiring images for two different temperatures, e.g. normal room temperature (300 K) and 1100 K from a hot air blower:

$$E^{\mathrm{H}^1}(\mathrm{air}) = f(T_1)OS + Q\,, \tag{A4}$$

$$E^{\mathrm{V}^1}(\mathrm{air}) = f(T_1)OS + Q/p\,, \tag{A5}$$

$$E^{\mathrm{H}^2}(\mathrm{air}) = f(T_2)OS + Q\,, \tag{A6}$$

$$E^{\mathrm{V}^2}(\mathrm{air}) = f(T_2)OS + Q/p\,. \tag{A7}$$

The ratio

$$r = f(T_1)/f(T_2) \tag{A8}$$

can be calculated for a given spectral interval from theoretical O/S branch spectra as shown in Fig. 7. So the factor p

is obtained from (A4–A8):

$$p = [E^{H^1}(\text{air}) - rE^{H^2}(\text{air})]/[E^{V^1}(\text{air}) - rE^{V^2}(\text{air})]\,. \quad \text{(A9)}$$

(Instead of using the temperature dependence of $f(T)$, as demonstrated here, the factor p could also be determined from two different integration intervals applied to a measurement in room air, but this is only precise at higher temperature when the O/S branches are wide.) Then the Q branch intensity is calculated from (A3). From Q the density is obtained via the cross-section measurement in room air and the theoretical temperature dependence of the cross-section. For temperature determination from a Stokes/anti-Stokes ratio the anti-Stokes emission is treated in an analogous way.

References

1. A. Leipertz: Temperaturbestimmung in Gasen mittels linearer und nichtlinearer Raman-Prozesse. Postdoctoral Thesis, Ruhr-Universität Bochum (1984)
2. A.R. Masri, R.W. Bilger, R.W. Dibble: Combust. Flame **71**, 245 (1988)
3. M.S. Mansour, R.W. Bilger, R.W. Dibble: Combust. Flame **85**, 215 (1991)
4. T.S. Cheng, J.A. Wehrmeyer, R.W. Pitz: Combust. Flame **91**, 323 (1992)
5. S.P. Nandula, T.M. Brown, W.A. Cole, R.W. Pitz: 28th Joint Propulsion Conf., Nashville, TN (1992)
6. M. Lapp, C.M. Penney: *Laser Raman Gas Diagnostics* (Plenum, New York 1974)
7. S.M. Harvey: Ont. Res. Div. Rep. 79-286-K (1979)
   W.M. Roquemore, P.P. Yaney: Natl. Bur. Stand. Spec. Publ. **561**, 973 (1979)
8. A.C. Eckbreth: *Laser Diagnostics for Combustion Temperature and Species* (Abacus, Cambridge, MA 1988)
9. R.E. Setchell, D.P. Aeschliman: Appl. Spectrosc. **31**, 530 (1977)
10. W. Reckers, L. Hüwel, G. Grünefeld, P. Andresen: Appl. Opt. **32** (6), 907 (1993)
11. P. Andresen, G. Meijer, H. Schlüter, H. Voges, A. Koch, W. Hentschel, W. Oppermann, E. Rothe: Appl. Opt. **29**, 2392 (1990)
12. A. Koch, H. Voges, P. Andresen, H. Schlüter, D. Wolff, W. Hentschel, W. Oppermann, E. Rothe: Appl. Phys. B **56**, 177 (1993)
    W. Demtröder: *Laserspektroskopie, Grundlagen und Techniken* (Springer, Berlin, Heidelberg 1991)
13. A. Koch, A. Chryssostomou, P. Andresen, W. Bornscheuer: Appl. Phys. B **56**, 165 (1993)
14. J.-P. Sawerysyn, L.-R. Sochet, D. Desenne, M. Crunelle-Cras, F. Grase, M. Bridoux: In *Proc. 21st Int'l Symp. on Combustion* (The Combustion Institute, Pittsburgh, PA 1986) p. 491
15. J.R. Smith: SAE 800137 (1980)
    J.R. Smith: AIAA J-**18**, 118 (1979)
    S.-C. Johnston: SAE 800136 (1980)
16. G. Grünefeld: Private communication (1992)
17. P. Andresen, A. Bath, W. Gröger, H.W. Lülf, G. Meijer, J.J. terMeulen: Appl. Opt. **27**, 365 (1988)
18. M.M. Suschtschinskij: *Ramanspektren von Molekülen und Kristallen* (Heyden, Rheine 1974)
19. J.M. Flaud, C. Camy-Peyret, J.P. Maillard: Molec. Phys. **32**, 499 (1976)
20. T. Kadota, F.Q. Zhao, K. Miyoshi: SAE 900481 (1990)
21. O. Axner: Volvo Technol. Rep. **1/88**, 26 (1988)
    R. Shimizu, S. Matumoto, S. Furuno, M. Murayama, S. Kojima: SAE 10/92 (1992)
22. D.A. Long: *Raman Spectroscopy* (McGraw-Hill, New York 1977)